Influence of Innovative Porous Panels for Laminar Flow Control by Suction

Baptiste Egreteau, Arnaud Mure d'Alexis, Fabien Mery, Cécile Davoine

AIAA Aviation Forum and ASCEND co-located Conference Proceedings
29 July - 2 August 2024, Las Vegas, Nevada
AIAA AVIATION FORUM AND ASCEND 2024

10.2514/6.2024-3760

Influence of innovative porous panels for laminar flow control by suction

Baptiste Egreteau*, Arnaud Mure d'Alexis† and Fabien Méry‡
DMPE, ONERA, Université de Toulouse, 31000, Toulouse, France

Cécile Davoine§
DMAS, ONERA, Université Paris-Saclay, 92320, Châtillon, France

This paper presents the development process of a new porous titanium panel made by Spark Plasma Sintering (SPS) for laminar flow control by suction.

First, the development process of the porous panel is detailed. Small samples are produced by partial sintering in SPS. Then, they are characterised in permeability and surface roughness. Based on these data, the sample with the most interesting characteristics is chosen to be upscaled and make a full suction panel of 300×275mm**.**

Afterwards, this new SPS panel is mounted on an academic flat plate model equipped with suction chambers to delay the boundary layer transition by applying wall suction. It is ensured there is a bidimensional with zero pressure gradient grazing flow in a low disturbance wind tunnel, leading to a modal boundary-layer transition scenario. Then, the transition position is determined using hot-wire anemometry for three configurations: a smooth reference case, a case with the SPS panel without suction and a case with the SPS panel and wall suction. These results are then compared with a previous study led in the same flow conditions with microperforated titanium sheets as porous panel.

I. Nomenclature

TS wave	=	Tollmien-Schlichting wave
Tu	=	Turbulence level
PSD	=	Power spectral density
S_a	=	Surface average roughness
HLFC	=	Hybrid laminar flow control
K_p	=	Pressure coefficient
HW	=	Hot-Wire
u'_{rms}	=	root mean square value of the velocity's fluctuating part
U_∞	=	Mean flow velocity
U_e	=	Mean velocity outside the boundary layer

II. Introduction

In the context of climate change, interest in fuel consumption reduction technologies for commercial airliners has been renewed. A way to achieve it is to lower drag, which has 2 main origins: pressure and skin friction. Skin friction is directly related to the boundary layer, the flow region close to the wall with an important velocity decay in the wall-normal direction due to viscous effects. This boundary layer can be either laminar, which means the flow is smooth and regular, or turbulent, where the flow is chaotic, with many vortices developing. The key point is that the skin-friction coefficient is an order of magnitude higher for a turbulent boundary layer than a laminar one.

As the flow is turbulent for current airliners, substantial fuel spare could be obtained by extending the laminar region. It is achievable for lifting surfaces, and much research has been conducted on it since the 1950s as presented by Braslow

*PhD Student, ONERA / DMPE, baptiste.egreteau@onera.fr
†Master Student, ONERA / DMPE, arnaud.mure_dalexis@onera.fr
‡Research Fellow PhD, ONERA / DMPE, fabien.mery@onera.fr
§Research Fellow PhD, DMAS, ONERA, cecile.davoine@onera.fr

[1]. Indeed, the laminar-turbulent transition is triggered by the amplification of instabilities inside the boundary layer. For the bidimensional flows that we will be interested in, these waves were described by Tollmien [2] and Schlichting [3]. When these so-called Tollmien-Schlichting (TS) waves are significantly amplified, they interact with each other, and a turbulent breakdown begins. The idea, then, is to slightly modify the boundary-layer mean flow in the laminar region to alter the instabilities amplification and delay the transition location. A way to do so is to apply wall suction through a porous surface. Currently, these suction devices are implemented in Hybrid Laminar Flow (HLFC) systems as described by Krishnan *et al.* [4] or Young *et al.* [5].

A new porous panel for laminar flow control by suction is developed in this study. The requirements for these panels are as follows. They must be as permeable as possible to minimise the power required by the suction system. And they must disturb the grazing flow over them as little as possible. They can disturb the flow in two ways, either with surface defects or acoustic wall impedance effect. Historically, laminar flow control started with slotted surfaces as presented by Gregory [6]. However, these slots represent non-neglectable surface defects and do not spread suction homogeneously. Then, laminar flow control studies preferred using micro-perforated panels, and they still are the reference today with titanium sheets laser micro-drilled. However, these panels present some disadvantages. To control the flow efficiently, an evolutive suction distribution must be imposed chord-wise. Indeed, on aircraft wings, as the flow and, thus, the pressure strongly varies from the leading edge, the pressure drop between the outer flow and suction chambers must be continuously adapted in the chordwise direction. This can be done using a lot of chambers, as described by Krishnan *et al.*, or adjusting the porosity properties of the panel. Recently, a flight test with an HLFC concept on an A320 fin was performed [7] based on 20 suction chambers around the leading edge. Several main challenges for HLFC concept were highlighted in this paper. The major one writes: minimising system complexity, weight, and manufacturing cost. This minimisation can be achieved by reducing the number of chambers. Thus, the permeability of the panels should be evolutive. A recent solution proposed by Seitz *et al.* [8] is called TSSD (Tailored Skin Single Duct), where micro-perforated panels are associated with metallic meshes to control the pressure loss through the panel. The tailored combination enables variable permeability along the airfoil.

With the progress in powder metallurgy, new opportunities can be explored to make near-net shape panels with scalable porosity and more complex pore networks that will influence the materials' permeability and acoustic response. Another possibility is thus to use panels made of sintered metal powders. Indeed, some tests of laminar flow control with sintered porous panels have already been made. Braslow *et al.* led a pioneering study on laminar flow control with a porous sintered bronze skin [9]. It proved incomplete sintered metal could be effective but encountered issues due to surface roughness and clogging because of sandblasting. More recently, Egreteau *et al.* [10] also performed a flow control experiment with a porous sintered stainless steel made by the MOTT firm. This panel proved to be at least as efficient as reference laser micro-drilled titanium sheets with more limited disturbance due to acoustic impedance. Partial densification by sintering seems to be an interesting manner of manufacturing porous panels. Among all sintering processes, a quick and anisotropic one would be preferred. This is why Spark Plasma Sintering (SPS) is used here.

The aim of this study is to manufacture an innovative porous panel and test it in a research wind tunnel. The porous materials will be made by SPS. It is then carefully characterised and compared with reference titanium sheets. Afterwards, the most promising sample will be upscaled to make a full suction panel implemented on an academic flat plate model with suction chambers. The flat plate will be placed in an open return subsonic research wind tunnel with a low disturbance level. Boundary-layer laminar-turbulent transition position will be measured to determine the performance of this new porous panel.

III. Development of a porous panel by SPS

This section details the development of the porous panel, with the manufacturing process of the samples, the characterisation process and the upscaling step to produce a larger panel.

A. Partial densification by SPS

The procces used is called spark plasma sintering (SPS). It is a sintering process (illustrated in Figure 1a), which means it consolidates powder by diffusion in solid state. SPS working principle is the following one. Metal powder is loaded in a cylindrical graphite die sealed with conductive carbon paper. This die is placed in a hydraulic press with graphite pistons so that high pressure and electric current can be applied simultaneously in a controlled atmosphere. Due to the Joule effect, the current passing through the die and the powder increases the temperature. This heats the powder from inside and outside.

As presented by Dudina *et al.* [11], there are many ways to make porous samples by SPS. Here, the partial

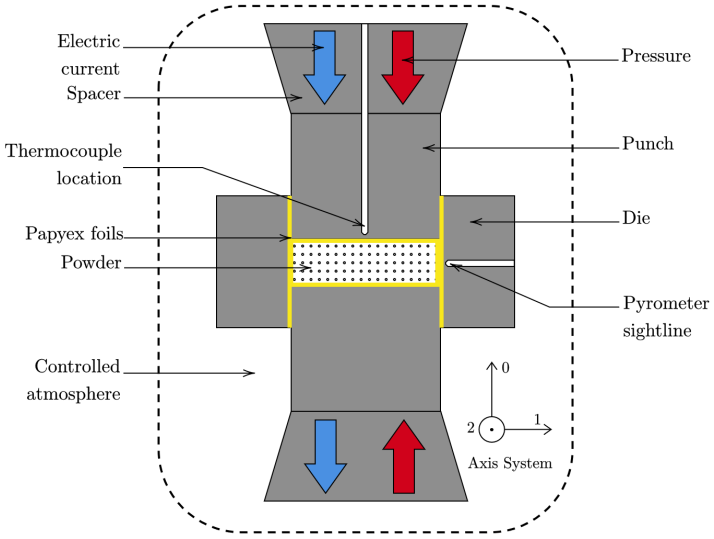

(a) Diagram of spark plasma sintering plant

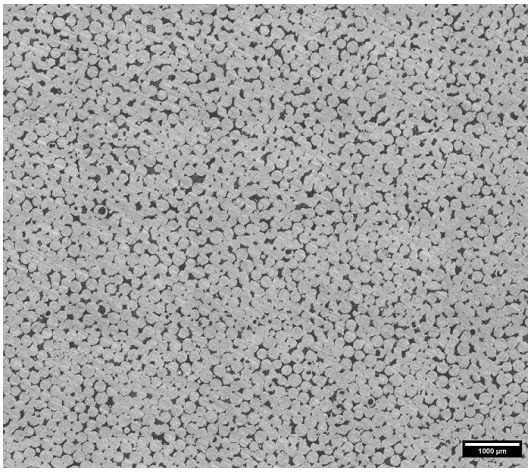

(b) Optical microscope view, along to the pressure direction (axis 0), of a porous sample made by SPS (partial sintering) after polishing

Fig. 1 Partial densification by SPS

densification method is preferred for simplicity. This means sintering is conducted in conditions (time, pressure, temperature) that do not allow complete powder densification. Thus, if the remaining pores are connected in an open network, it can draw air through. Moreover, as the electric current and the pressure are uniaxially applied, an anisotropic porous network could be formed.

As many parameters could influence samples permeability, it has been chosen to use only temperature (between 750 and 850°C) and pressure (between 5 and 20 MPa) as design variables. All other parameters were set to the following values :

- Die: cylindrical, 36 mm diameter
- Powder: 15 g of spherical titanium alloy (Ti64), 200-250 µm diameter
- Heating rate: 100°C/min
- Dwell time: 5 min

A coarse powder was chosen to have large spaces between powder particles thus ensuring a percolating porous network after sintering. The quantity of powder was chosen to make 3 to 5 mm thick pastilles to have a compromise between good sintering conditions and moderate pressure drop for permeability evaluation. An example of the structure of the sample is visible on Figure 1b

B. Characterisation protocol

For laminar flow control, porous panels should have low pressure loss to minimise suction power. These pressure losses can be deduced from the material's permeability. The panels should also over-amplify TS waves as little as possible. Over-amplification of TS waves can be caused by surface roughness [12], or acoustic effects modeled by acoustic impedance [13]. This is why our porous materials' permeability and roughness have been measured.

1. Permeability

Permeability is measured thanks to an experimental setup presented on Figure 2. An airflow, injected in a plenum, goes through the sample by a known injection diameter. The pressure drop from each side of the sample ($P_{\text{atmo}} - P_1$) is measured and then the Darcy law (Equation1) is applied to extract the material's permeability.

$$-\frac{\Delta P}{L} = \frac{\mu}{K_D} V \tag{1}$$

With:

- ΔP [Pa]: Pressure difference on each side of the porous medium

- L [m]: Porous medium thickness
- μ [kg m^{-1} s^{-1}]: Fluid dynamic viscosity
- V [m s^{-1}]: Darcian velocity, calculated by dividing the volumetric flow rate by the cross-sectional area.
- K_D [m^2]: Permeability, associated to viscous effects, in Darcy regime

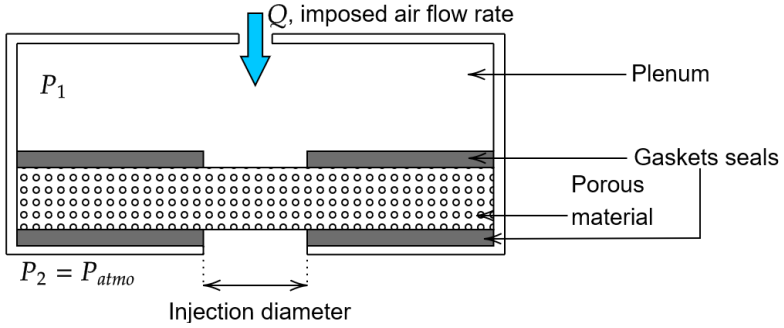

Fig. 2 Sketch of the permeability test bench

The permeability measurements are shown in Figure3. The values reachable with SPS (between 5×10^{-14} m^2 and 1×10^{-11} m^2 for the manufacturing conditions set out above) matched with the ones of classical micro-drilled titanium sheets usually used for HLFC purpose (about 1×10^{-12} m^2 measured on our bench). Moreover the influence of sintering temperature and pressure are clearly visible: the higher they are, the lower the permeability.

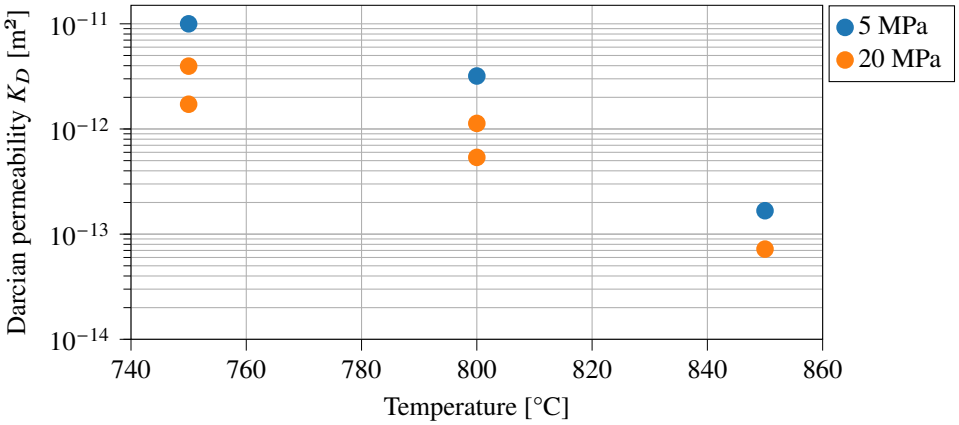

Fig. 3 Darcian permeability measured for all samples

2. Surface roughness

Surface roughness can be regarded as the quality of a surface not being smooth and is defined as the deviations in the direction of the normal vector of a real surface from its ideal form. It seems obvious that the surface roughness of an aircraft is important in terms of aerodynamic performance. In wind tunnel testing, to take account of the scale down, the roughness of a model is essential to assess performance, particularly in the transonic regime correctly. Vorburger *et al.* [14] proposed a study to measure the roughness of the wind tunnel model. This article is dedicated to a model for the National Transonic Facility (NTF), which is a transonic wind tunnel. Typical, admissible roughness should be less than 0.2µm corresponding to a mirror-polished steel. Based on Nikuradse's pipe measurement, a typical admissible roughness k should satisfy $k \leq \dfrac{100}{Re_{uni}}$ with the unit Reynolds number $Re_{uni} = U_\infty/\nu$ with U_∞ the velocity of the flow and ν the kinematic viscosity. With $\mathrm{Re_{uni}}=2.6 \times 10^6 \mathrm{m}^{-1}$, we have $k \leq 38.4$µm. Moreover, it is a critical factor in boundary layer transition, as roughness boosts the wave amplification that triggers the transition. Von Doenhoff & Horton[15] and more recently Ducaffy [12] emphasised the impact of the distributed roughness. There are many values to quantify it (average roughness, quadratic mean, maximum peak/valley height, ...). In our case, roughness was

measured with an optical profilometer (Brukers Alicona Infinite Focus) using a focus variation method, following the ISO25178 norm (description of surface texture parameters).

For SPS samples, roughness was first measured on samples that were polished to remove the carbon paper that stuck to them. This gave very low S_a (between 0.8 and 4.7 µm). However, this polishing step would be difficult on larger panels without introducing surface defects. This is why another sample preparation procedure was tested to prevent carbon paper from sticking to the samples. The new S_a was about 28µm. As intended without polishing, average roughness is far higher because the powder particles tops were not removed. Nevertheless, this opportunity to avoid polishing large surfaces is profitable for the simplicity of the process.

C. Porous panels upscaling

After this characterisation protocol, the preferable manufacturing parameters were chosen. The most promising SPS sample is made at 800°C and 20MPa. Indeed, it offers a reasonable permeability: 5×10^{-13} - 10^{-12}m^2, where micro drilled panels are between 10^{-12} and 5×10^{-12}m^2 for an acceptable thickness (2mm).

To reproduce this sample at a larger scale, a fine prediction of the thermal field inside it during manufacturing is required. This modelisation allows the optimisation of the die geometry to minimise the temperature gradient inside the sample during manufacturing, which would result in an inhomogeneous sintering. This was done in collaboration with Norimat. The conclusion was that 3 samples of 300mm diameter and 2mm thickness made with 456g of Ti64 powder were needed to cover the suction region. The temperature difference between the sample's centre and edges was kept at 25°C with a maximal current intensity of 24kA. After manufacturing, it was determined that the thickness was not regular. It was 2.5mm at the centre and 1.9mm on the edges. These samples were then cut into 100×275mm panels and assembled on a frame visible in Figure 4. Samples were constrained while being assembled to minimise surface defects on the wetted side.

The roughness of the panels was measured as detailed previously. S_a values were the same as the one measured on the small scale sample: $S_a \in [26 - 30]$µm.

Fig. 4 SPS panels assembled on its frame

IV. Overview of the experimental method

A. Experimental facility

The experiment is taking place in ONERA's TRIN-2 research wind-tunnel, illustrated on Figure 5. It is an open-return wind-tunnel with a test section 0.4x0.3x1.5m and a converging nozzle. The converging nozzle has an area ratio of 16. It works in incompressible regime (maximum velocity 48 m/s without a model) at atmospheric conditions. The diverging nozzle is treated with a noise reduction chicane (not represented in Figure 5) between the test section and the fan to prevent parasite waves from travelling upstream. The test section velocity and Reynolds number are determined with a Pitot tube and a total temperature probe (Type T thermocouple) located approximately 0.03 m from the test section ceiling and 0.15 m downstream of the pre-test section inlet.

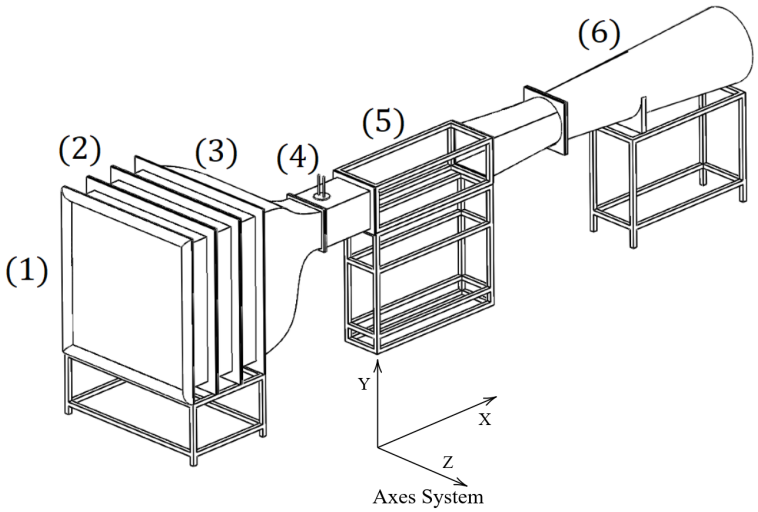

Fig. 5 ONERA TRIN2 wind-tunnel. (1) Collector; (2) Settling chamber; (3) Contraction; (4) Pre-test section; (5) Test Section and (6) Exhaust. (Reproduced from Jaroslawski [16])

All acquisitions are made with a Dantec Dynamics Streamline Pro system with a 90C10 module and a National Instruments CompactDAQ-9178 with two NI-9239 (built-in resolution of 24-bit) modules for voltage measurements and an NI-9211 (built-in resolution of 16-bit) module for temperature measurements.

Turbulence level inside wind tunnels is a key parameter driving the laminar-turbulent transition and, therefore, must be carefully measured [17] [18]. It has already been made by Methel [19] and Jaroslawski [20] for this facility using hot wire anemometry. This is why a similar protocol is followed here in the empty test section. The test section is divided into 6 positions in flow direction (x axis), and for each of them, the flow velocity is measured at 25 distinct locations (5 different on y and z axes) with a Dantec 55P11 probe. At each point, the hot-wire tension is acquired for 16s at 25kHz. This tension signal, E, is converted into U, the velocity component along flow direction, using a King's law [21]. Then, velocity power spectral density is computed by Welch method and integrated between 3Hz and 12.5kHz to compute the turbulence level according to equation 2:

$$Tu = \frac{u_{rms}}{U_\infty} = \frac{1}{U_\infty}\sqrt{\int_{f_{\min}}^{f_{\max}} \mathrm{PSD}_u(f)\,\mathrm{d}f} \tag{2}$$

With U_∞ the infinite upstream velocity, u the velocity component along x axis, u_{rms} its root mean square value, and f the frequency.

This allows us to plot a map of the turbulence level inside the empty test section for a unitary Reynolds number of $2.6 \times 10^6 \mathrm{m}^{-1}$. Figure 6 represents the Tu map at the test section inlet. It can be seen that far from the test section walls, where the model will be positioned (its lower side will be at y = 125mm and upper side at y = 160mm), Tu values remain low: they are inferior to 0.07% at the test section inlet and inferior to 0.1% over the full test section length). These results are comparable to Methel's ones [22], who measured Tu values below 0.18% at the test section centerline. The Tu values are higher near the test section floor and ceiling: about 0.24% at the test section inlet.

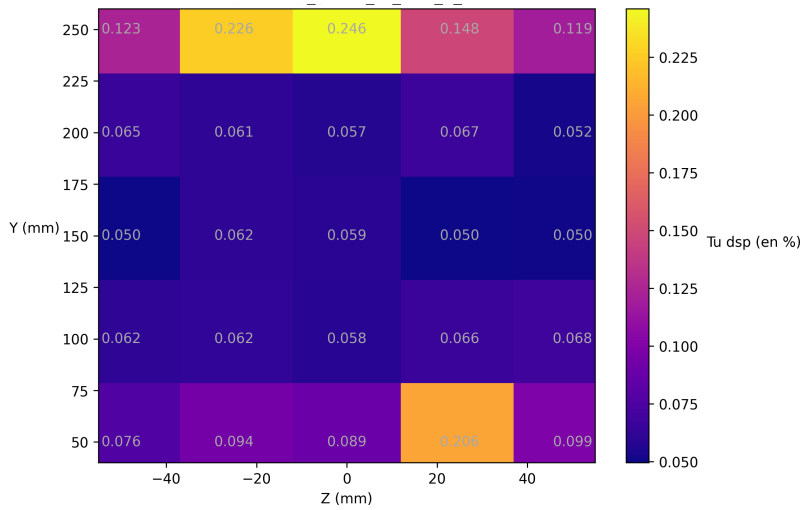

Fig. 6 Turbulence level measurements at the test section inlet (X=0mm) for a unit Reynolds number $\mathbf{Re_{uni}}$=$2.6 \times 10^6 \mathrm{m}^{-1}$

B. Model design and baseflow

The model is a flat plate as illustrated on Figure 7. It is intended to have a bidimensional grazing flow with no pressure gradient. It has been designed by taking inspiration from the one used by Methel [19]. It is 34.7mm thick, 400mm wide and 1456mm long, flap included (not visible on Figure 7). The leading edge shape is the same as the

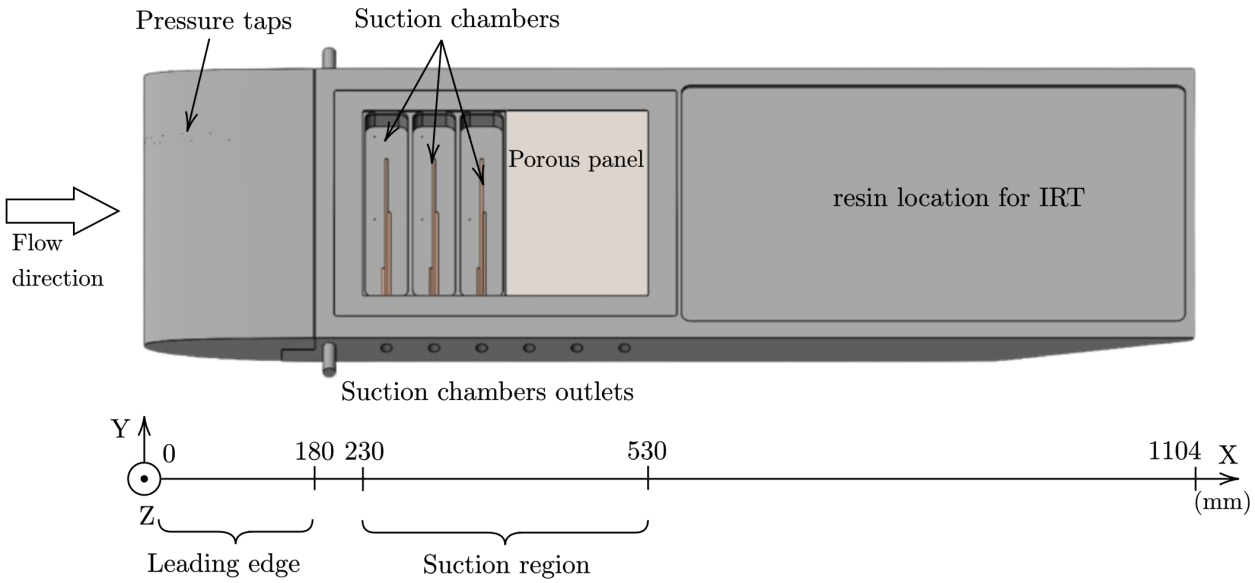

Fig. 7 CAD view of the flat plate model

previous model. It was optimised to minimise the overspeed peak [23]. It is 180mm long, thus having an aspect ratio of 10.2. It also has 20 pressure taps (3 on the lower surface and 16 on the upper one). In combination with an adjustable flap the stagnation point position is adjusted to ensure a minimal pressure gradient on the flat plate body. The pressure coefficient distribution along the leading edge was measured with an SVMtec PSC24 multichannel pressure sensor.

The model has 6 independent suction chambers. They are 45mm long, 275mm wide and separated by 5mm thick walls. The first suction chamber is placed at x = 230mm and the last ends at x = 530mm.

A 2mm-deep cavity downstream of the suction zone was designed so that a thermally insulating epoxy resin was poured in for IRT measurements.

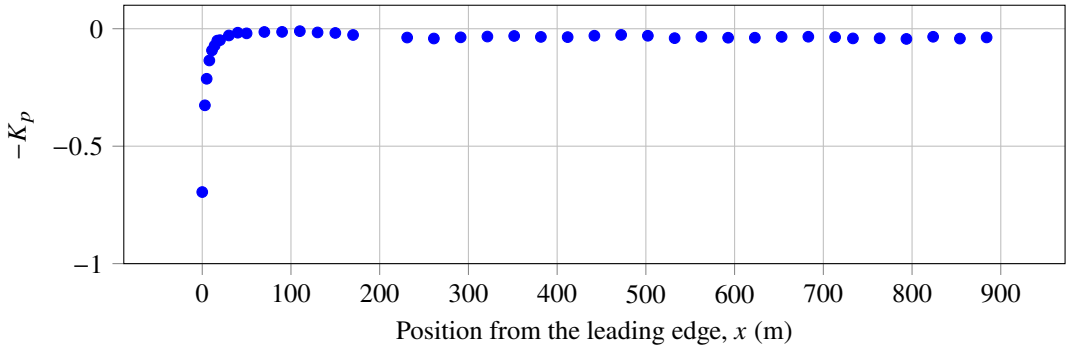

Fig. 8 Pressure coefficient distribution measured experimentally on the model upper side

Then, an initial test campaign was led to fully characterise the flow over the flat plate with a solid panel over the suction region. The purpose was to ensure a zero pressure gradient grazing flow starting laminar and transitioning to turbulence. The method to detect the location of the transition is also detailed.

The turbulence level was measured 20mm upstream of the model's leading edge. The Tu is computed the same way as in the empty test section. Its values are displayed in Figure9a and the PSD used to compute the Tu at $z = -50$mm is shown in Figure9b. The Tu values remain below 0.18%.

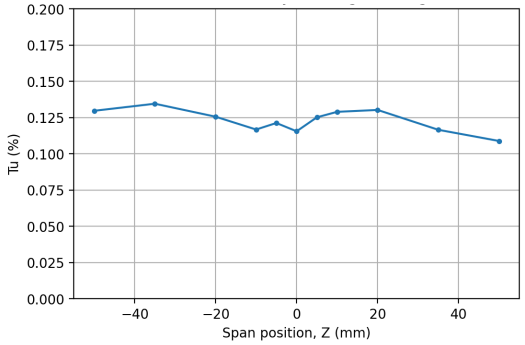

(a) Turbulence level 20 mm **upstream of the leading edge**

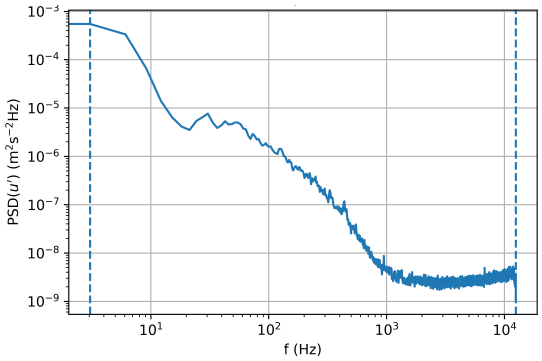

(b) PSD of the velocity signal at $z = -50$ mm **with the integrated frequency range for RMS computation (dashed lines).**

Fig. 9 Turbulence level measurements at $Re_{/1m}$=$2.6 \times 10^6 m^{-1}$, 20 mm **upstream the leading edge. RMS values computed from PSD integrated from** 3Hz **to** 12 5kHz**.**

The pressure coefficient, K_p distribution for Re_{uni}=$2.6 \times 10^6 m^{-1}$ is plotted in Figure 8. The leading edge K_p ($x \in [0, 180]$mm) were computed from the pressure taps. The following ones over the flat plate body were computed from hot wire measurements outside the boundary layer, assuming the flow is incompressible as the Mach number is about 0.1. The data shows there is no pressure gradient over the flat plate body (*i.e.* x>180mm) for a flap angle of $-2.7°$.

Vertical probings were then performed in the region expected laminar. The mean velocity profiles are then compared with Blasius autosimilar solution as shown in Figure 10, with η being the dimensionless variable of Blasius: $\eta = \frac{y\sqrt{Re_x}}{x}$. The shape factor was computed for each profile, with values about 2.02. This value confirms that the boundary layer is laminar in this region as the theoretical shape factor of the Blasius profile is 2.6.

Longitudinal traverse probings were conducted at many span positions to determine the boundary-layer laminar-turbulent location. These measurements were made with a Dantec 55P15 probe, 400µm above the wall. The way the transition location is detected is detailed in Figure 11 for the probing on the centerline. At each point, the RMS level is computed following Equation 2 taking frequencies from 3Hz to 12 5kHz. Then, an exponential curve is fitted on

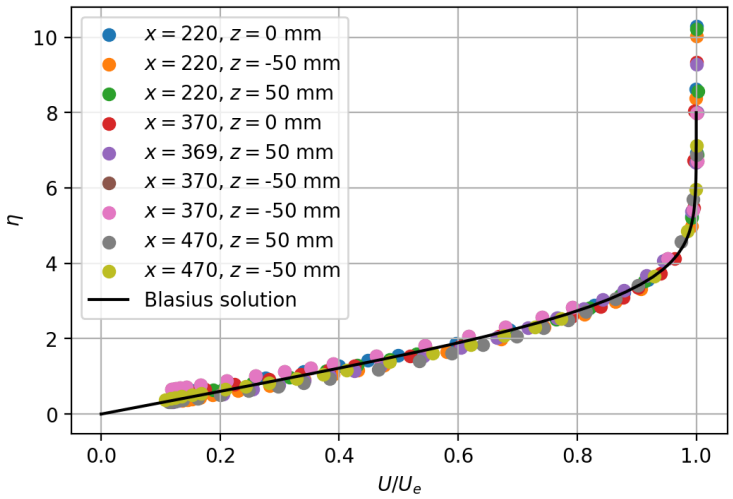

Fig. 10 Comparison between Blasius profile and experimental velocity profile measurements

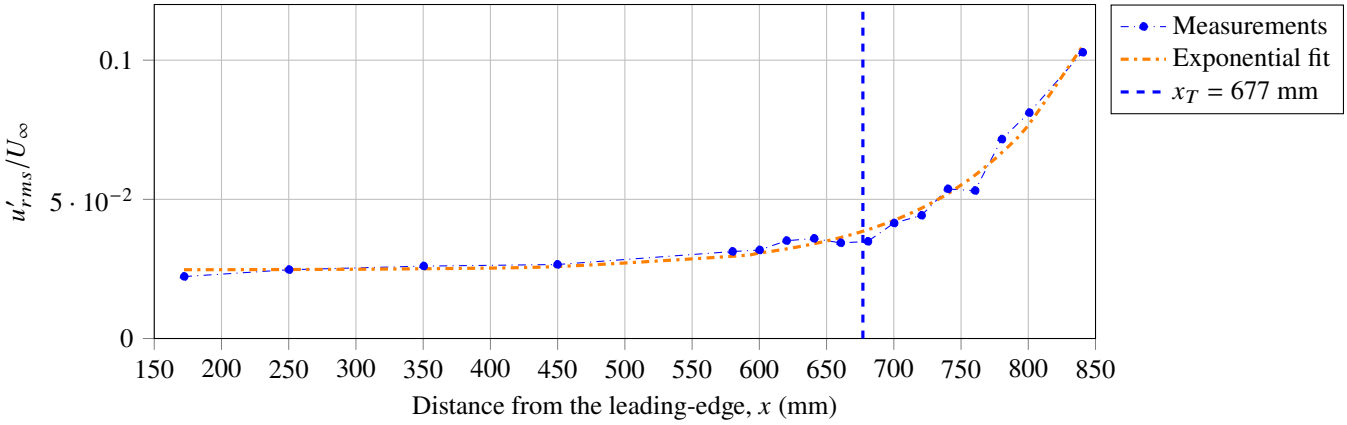

Fig. 11 Transition position detection on the centerline at Re_{uni}=$2.6 \times 10^6 m^{-1}$ and y=400µm altitude. RMS values computed from PSD integrated from 3Hz to 12.5kHz. Detection threshold set at $1.5 \times 10^{-4} mm^{-1}$

the chordwise RMS distribution. Finally, the transition location is detected when the fitted curve's gradient reaches $1.5 \times 10^{-4} mm^{-1}$.

V. Effect of suction through the SPS porous panel on the boundary layer transition

A. Studied configurations

This study is based on Methel's one [22] about the experimental characterisation of the laminar-turbulent transition of a sucked boundary layer. First, the transition location was measured on a smooth configuration (*i.e.* with a smooth and solid panel covering the suction region), a configuration with a microdrilled titanium panel without applying suction and 3 configurations with a microdrilled titanium panel and applying suction of $0.4 gs^{-1}$ with different suction distribution over the suction chambers. Then, the effects of surface defects on boundary layer transition with wall-suction were studied. Here, the configurations that we are interested in are the smooth one, the one with a porous panel without suction and the one called full suction, applying a $0.4 gs^{-1}$ suction distributed over all suction chambers.

These configurations are reproduced using the SPS panel instead of the microdrilled titanium one and in the same flow conditions, which means in the same wind-tunnel and at the same unit Reynolds number (Re_{uni}=$2.6 \times 10^6 m^{-1}$). A

notable difference from the previous study is the ability to probe across the test section for 50mm on either side of the centerline. This will allow us to ensure the transition's bidimensionality over the model's span. For each configuration, longitudinal traverse probings will be made at 9 different span positions ($z = [0, \pm5, \pm10, \pm30, \pm50]$mm).

Table 1 Reference and studied configurations

Configuration name	Panel used	Suction flow rate[gs^{-1}]	Configuration description
Methel [22, 23], smooth	solid	0	Methel's reference case with a solid panel over the suction region
Methel [22, 23], no suction	microdrilled sheet	0	Methel's reference case with a microdrilled panel over the suction region and without suction
Methel [22, 23], full suction	microdrilled sheet	0.4	Methel's reference case with a microdrilled panel over the suction region and a distributed suction
Smooth	solid	0	Case with a solid panel over the suction region on the new model
SPS, no suction	SPS	0	Case with the SPS panel over the suction region on the new model and without suction
SPS, full suction	SPS	0.4	Case with the SPS panel over the suction region on the new model and a distributed suction

B. Transition position results

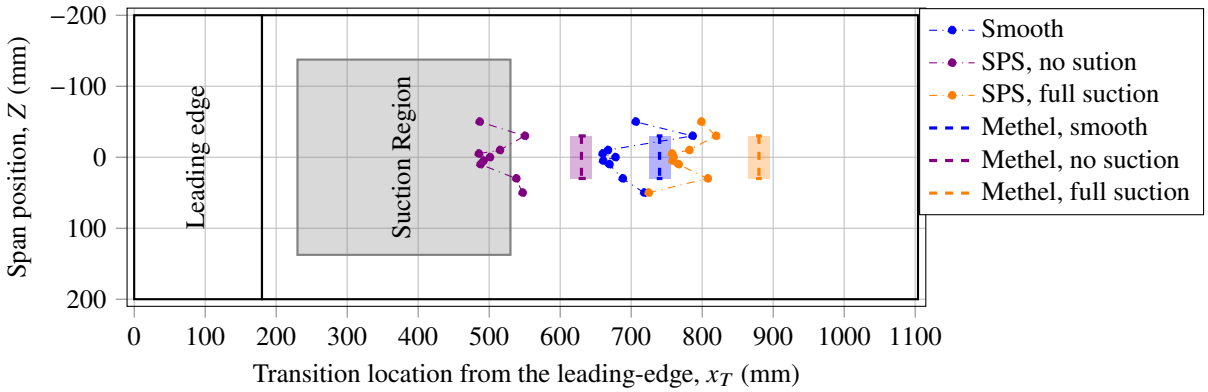

(a) Overview to the whole flat plate

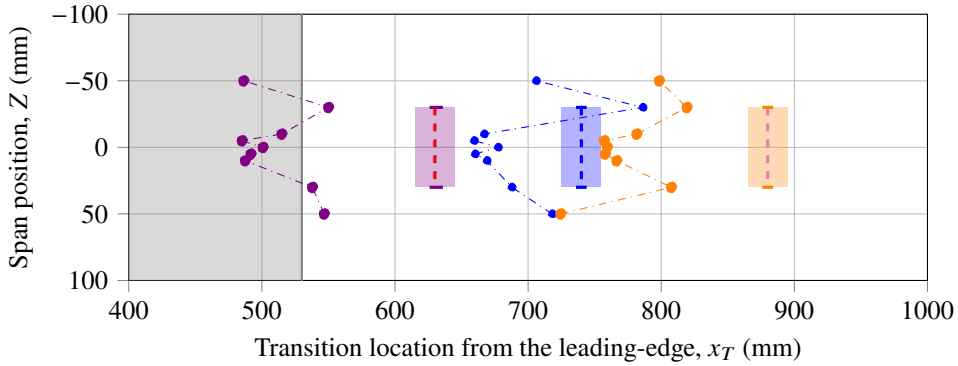

(b) Magnified view

Fig. 12 Transition locations for all configurations at Re_{uni}=$2.6 \times 10^6 m^{-1}$ and y =400 µm altitude. RMS values computed from PSD integrated from 3 to 12.5 kHz. Detection threshold set at $1.5 \times 10^{-4} mm^{-1}$.

The transition locations measured for the 3 configurations are plotted in Figure 12. The reference transition locations from Methel [22] are also plotted in dashed lines. The transition line of the smooth case is not bidimensional over the entire span. Nevertheless, transition locations for $z \in [-10, 50]$mm are within a 50mm range. This leads us to conclude that the flow can be considered bidimensional in this region around the centerline with a mean transition position at 677mm. This is 63mm upstream of the transition location detected by Methel with similar model and flow conditions. In Figure12, Methel's transition locations are represented with dashed lines on the mean value with a colour band accounting for uncertainty.

A similar behaviour is observed on the transition line for the SPS no suction case with a mean transition location around the centerline at 509mm. It is 168mm upstream of the smooth configuration. This transition promotion should be due to TS waves over-amplification. Two phenomena could have over-amplified the TS waves: surface roughness and an acoustic impedance effect. Ducaffy [12] studied the effect of distributed surface roughness and determined that for high roughness values, the TS waves are locally overamplified over the rough area compared with a smooth case. As a result, TS waves reach the critical amplification rate that triggers the boundary layer transition earlier. It is very likely that this phenomenon occurs over the SPS panel, as its average roughness S_a is about 30µm, whereas the rest of the model, $S_a = 0.25$µm. It has been recently demonstrated by Rouviere *et al.* [13] that a boundary layer developing over a porous flat plate transitions earlier to turbulence than on a solid one. This paper examines the effect of a perforated panel without suction as an impedance boundary condition destabilising the TS waves responsible for the laminar to turbulent transition. The promotion of transition when the boundary layer developed over the perforated panels has been demonstrated experimentally. This effect is due to an impedance condition coupling the wall-normal velocity and the pressure fluctuations at the wall. As the SPS panel is also porous, it should behave in a similar manner to microperforated sheets. This transition location is 171mm upstream of Methel's no suction case.

Finally, for the full suction configuration, the transition line is still bidimensional for $z \in [-10, 30]$mm with a mean transition location of 765mm. In this configuration, the transition is delayed downstream of 256mm compared with the no suction case and 88mm compared with the smooth case. However, it is still 115mm upstream of Methel's full suction configuration. This gap, which is twice as high as the one between the smooth configurations, might be due to SPS roughness, which is far higher than that of micro-drilled sheets.

An example of the results provided by the longitudinal traverse probings with detected transition positions is shown in Figure13 for each configuration on the centerline. Whereas Figure14 provides the PSD computed at each point of the longitudinal traverse probing on the centerline for the smooth configuration. A bump that increases with x value can be seen around 600Hz. This should be the spectral signature of the TS waves amplifying in the boundary layer, based on Methel's analysis for the same geometry and flow conditions [22, 23].

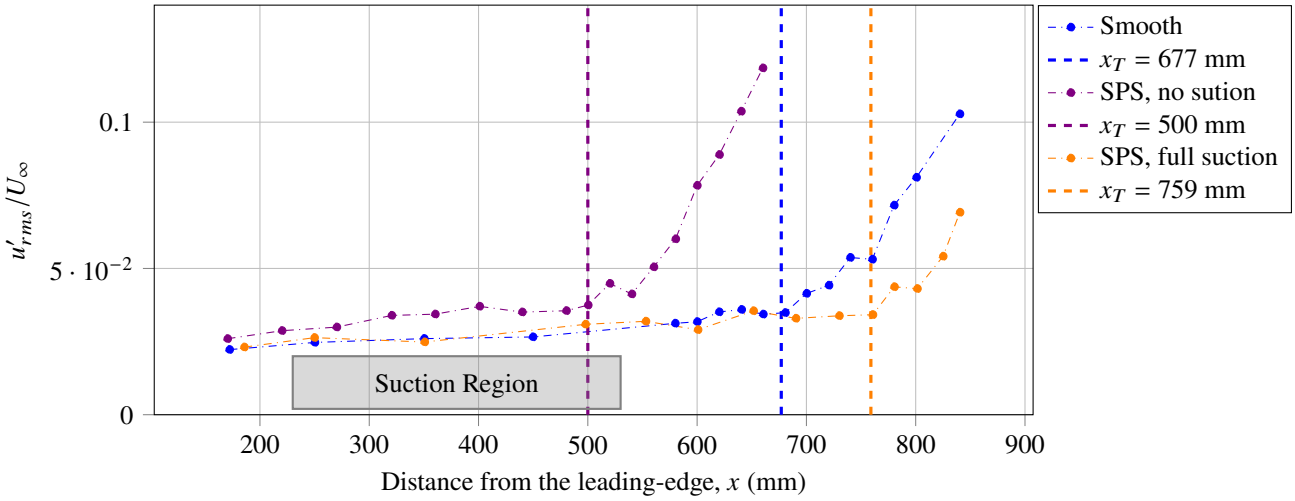

Fig. 13 Longitudinal traverse probings on the centerline at Re_{uni}=$2.6 \times 10^6 m^{-1}$ and y =400µm altitude. RMS values computed from PSD integrated from 3 to 12.5kHz. Detection threshold set at $1.5 \times 10^{-4} mm^{-1}$

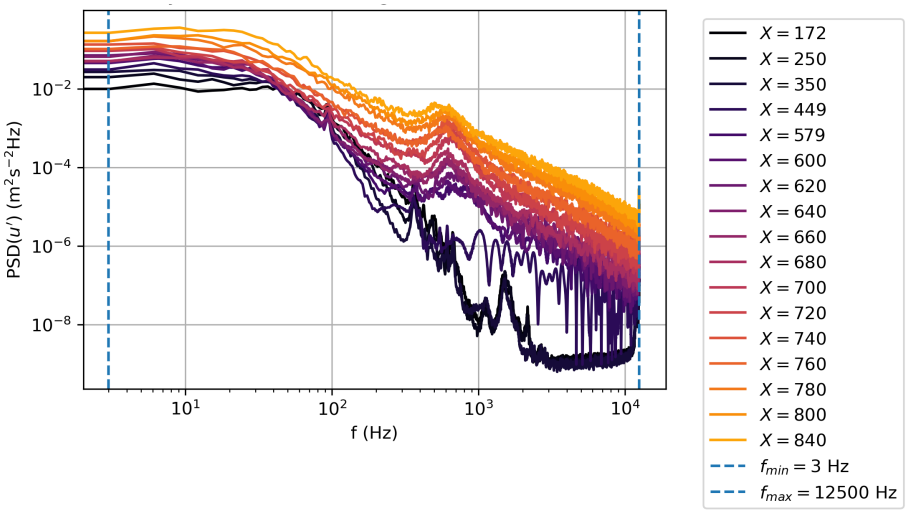

Fig. 14 PSD computed at each point of the longitudinal traverse probings on the centerline for the smootch configuration at Re_{uni}=$2.6 \times 10^6 m^{-1}$ and y =400µm altitude.

VI. Conclusion

To conclude, this paper presented the development process of a new porous titanium panel made by SPS for laminar flow control by suction. Through partial densification, it is possible to make thin porous samples (2mm thick) with permeability values ($[5 \times 10^{-14}, 10^{-11}]m^2$) comparable with micro-drilled sheets ($[10^{-12}, 5 \times 10^{-12}]m^2$ for a 1mm thickness) that are the reference panel for laminar flow control by suction. The roughness of the gross samples was high ($S_a \approx 28$µm), but it could be improved to $S_a \approx 2$µm with an adequate polishing that did not clog the pores on the surface. Afterwards, the most promising sample was successfully reproduced on a larger scale through a numerical modelisation of its manufacturing to minimise temperature gradients. The production of 3 discs of 300mm diameter and 2 mm thick enabled us to make a porous panel of 300×275mm. Further work could then be carried out to produce the porous panel in a single part. This would prevent potential surface defects due to imperfect assembling.

Afterwards, this new SPS panel was mounted on an academic flat plate model equipped with suction chambers to delay the boundary layer transition by applying wall suction. It was ensured that there was a bidimensional with zero pressure gradient grazing flow in a low disturbance wind tunnel, leading to a modal boundary-layer transition scenario. The transition position was determined using HW anemometry for three configurations: smooth, SPS no suction and SPS full suction. For the SPS no suction case, the transition settles upstream of the smooth one. This should be due to an overamplification of TS waves because of a combination of surface roughness and wall impedance effect over the SPS panel. When applying wall suction in the SPS full suction configuration, the transition settles downstream of the smooth case.

This study proved that porous panels made by SPS are suitable for boundary layer transition control by suction. Nevertheless, the performances are not as good as the ones of reference micro-drilled sheets used by Methel [22, 23] in the same flow conditions. Nevertheless, there are avenues for improvement involving reducing roughness and assembly defects in porous panels.

Acknowledgments

This work has been partially funded by the NACOR project, within the frame of the Joint Technology Initiative JTI Clean Sky 2, AIRFRAME Integrated Technology Demonstrator platform being part of the Horizon 2020 Research and Innovation framework program of the European Commission (Grant Agreement N° 945521).

References

[1] Braslow, A. L., *A history of suction-type laminar-flow control with emphasis on flight research*, 13, NASA History Division, Office of Policy and Plans, NASA Headquarters, 1999.

[2] Tollmien, W., "Über die entstehung der turbulenz. Nachr. Ges. Wiss. Göttingen 21–24," *English translation 1931, NACA TM609*, 1929. https://doi.org/10.1007/978-3-662-33791-2_4.

[3] Schlichting, H., "Über das ebene Windschattenproblem," *Ingenieur-Archiv*, Vol. 1, No. 5, 1930, pp. 533–571. https://doi.org/10.1007/bf02079870.

[4] Krishnan, K. S. G., Bertram, O., and Seibel, O., "Review of hybrid laminar flow control systems," *Progress in Aerospace Sciences*, Vol. 93, 2017, pp. 24–52. https://doi.org/10.1016/j.paerosci.2017.05.005.

[5] Young, T., Humphreys, B., and Fielding, J., "Investigation of hybrid laminar flow control (HLFC) surfaces," *Aircraft Design*, Vol. 4, No. 2-3, 2001, pp. 127–146. https://doi.org/10.1016/S1369-8869(01)00010-6.

[6] Gregory, N., "Research on suction surfaces for laminar flow," *Boundary layer and flow control*, 1961, pp. 924–960.

[7] Schrauf, G., and von Geyr, H., "Hybrid Laminar Flow Control on A320 Fin: Retrofit Design and Sample Results," *Journal of Aircraft*, Vol. 58, No. 6, 2021, pp. 1272–1280. https://doi.org/10.2514/1.C036179.

[8] Seitz, A., Horn, M., Barklage, A., Scholz, P., Badrya, C., and Radespiel, R., "Wind Tunnel Verification of Laminar Boundary Layer Control TSSD Concept," *AIAA Aviation 2022 Forum*, 2022, p. 3552.

[9] Braslow, A. L., Burrows, D. L., Tetervin, N., and Visconti, F., "Experimental and Theoretical Studies of Area Suction for the Control of the Laminar Boundary Layer on an NACA 64a010 Airfoil," Tech. Rep. NACA-TR-1025, NACA, Jan. 1951. URL https://ntrs.nasa.gov/citations/19930092080.

[10] Egreteau, B., Methel, J., Mery, F., Vermeersch, O., Davoine, C., Forte, M., and Thomas, M., "Control of laminar turbulent transition using wall suction through a porous metal foam," *56th 3AF International Conference on Applied Aerodynamics*, Toulouse, 2022, p. 8.

[11] Dudina, D., Bokhonov, B., and Olevsky, E., "Fabrication of Porous Materials by Spark Plasma Sintering: A Review," *Materials*, Vol. 12, No. 3, 2019, p. 541. https://doi.org/10.3390/ma12030541.

[12] Ducaffy, F., Forte, M., Vermeersch, O., and Piot, E., *An experimental study of the effects of surface roughness on the laminar-turbulent transition of a 2D incompressible boundary-layer*, ???? https://doi.org/10.2514/6.2021-0247.

[13] Rouviere, A., Méry, F., Methel, J., Vermeersch, O., and Forte, M., "Experimental and Numerical Study on Wall Impedance Effects on Tollmien–Schlichting Waves," *AIAA Journal*, 2021, pp. 1–12. https://doi.org/10.2514/1.J060536.

[14] Vorburger, T. V., McLay, M. J., Scire, F. E., Gilsinn, D. E., Giauque, C. H. W., and Teague, E. C., "Surface roughness studies for wind tunnel models used in high Reynolds number testing," *Journal of Aircraft*, Vol. 23, No. 1, 1986, pp. 56–61. https://doi.org/10.2514/3.45266.

[15] Von Doenhoff, A., and Horton, E., *A Low Speed Experimental Investigation of the Effect of a Sandpaper Type of Roughness on Boundary Layer Transition*, NACA R-1349, NACA, 1958. URL https://books.google.fr/books?id=WLwevwEACAAJ.

[16] Jaroslawski, T., "Transition dans les bulles de décollement laminaires sur les voilures fixes et tournantes à faible nombre de Reynolds," Ph.D. thesis, 2023.

[17] Owen, F. K., and Owen, A. K., "Measurement and assessment of wind tunnel flow quality," *Progress in Aerospace Sciences*, Vol. 44, No. 5, 2008, pp. 315–348. https://doi.org/10.1016/j.paerosci.2008.04.002, URL https://linkinghub.elsevier.com/retrieve/pii/S0376042108000286.

[18] Hunt, L., Downs, R., Kuester, M., White, E., and Saric, W., "Flow Quality Measurements in the Klebanoff-Saric Wind Tunnel," *27th AIAA Aerodynamic Measurement Technology and Ground Testing Conference*, American Institute of Aeronautics and Astronautics, Chicago, Illinois, 2010. https://doi.org/10.2514/6.2010-4538, URL https://arc.aiaa.org/doi/10.2514/6.2010-4538.

[19] Methel, J., "An Experimental Investigation of the Effects of Surface Defects on the Laminar-Turbulent Transition of a Boundary Layer with Wall Suction," Ph.D thesis, ISAE-Supaéro, Université de Toulouse, Nov. 2019.

[20] Jaroslawski, T., Forte, M., Vermeersch, O., Moschetta, J.-M., and Gowree, E. R., "Disturbance growth in a laminar separation bubble subjected to free-stream turbulence," *Journal of Fluid Mechanics*, Vol. 956, 2023, p. A33. https://doi.org/10.1017/jfm.2023.23.

[21] Bruun, H. H., "Hot-wire anemometry: principles and signal analysis," *Measurement Science and Technology*, Vol. 7, No. 10, 1996, p. 024.

[22] Methel, J., Vermeersch, O., Forte, M., and Casalis, G., "Experimental Characterization of the Laminar-Turbulent Transition of a Sucked Boundary Layer due to Surface Defects in a Two-Dimensional Incompressible Flow," *2018 Flow Control Conference*, American Institute of Aeronautics and Astronautics, Atlanta, Georgia, 2018. https://doi.org/10.2514/6.2018-3214, URL https://arc.aiaa.org/doi/10.2514/6.2018-3214.

[23] Methel, J., Forte, M., Vermeersch, O., and Casalis, G., "An experimental study on the effects of two-dimensional positive surface defects on the laminar–turbulent transition of a sucked boundary layer," *Experiments in Fluids*, Vol. 60, 2019, pp. 1–18.